Int J Thermophys (2012) 33:1989–1995
DOI 10.1007/s10765-012-1285-y

Thermal Coherence Tomography: Depth-Resolved Imaging in Parabolic Diffusion-Wave Fields Using the Thermal-Wave Radar

N. Tabatabaei · A. Mandelis

Received: 10 February 2012 / Accepted: 14 August 2012 / Published online: 14 September 2012

Abstract Energy transport in diffusion-wave fields is gradient driven and therefore diffuse, yielding depth-integrated responses with poor axial resolution. Using matched filter principles, a methodology is proposed enabling these parabolic diffusion-wave energy fields to exhibit energy localization akin to propagating hyperbolic wave fields. This not only improves the axial resolution, but also allows for deconvolution of individual responses of superposed axially discrete sources, opening a new field of depth-resolved subsurface thermal coherence tomography using diffusion waves. The depth-resolved nature of the developed methodology is verified through experiments carried out on phantoms and biological samples. The results suggest that thermal coherence tomography can resolve deep structural changes in hard dental and bone tissues, allowing for remote detection of early dental caries and potentially early osteoporosis.

Keywords Dental caries · Matched filtering · Osteoporosis · Phase modulation · Thermal coherence tomography · Thermophotonics

1 Introduction

Unlike hyperbolic traveling waves, such as acoustic or optical waves, the physics of diffusive thermal waves is governed by the parabolic heat diffusion equation and in accordance to Fickian principles. An immediate consequence of the gradient-driven principle is the lack of wave fronts and the diffuse depth-integrated (rather than depth-resolved) transport of power through the medium, leading to poor diffusive axial

N. Tabatabaei · A. Mandelis (✉)
Center for Advanced Diffusion-Wave Technologies, Department of Mechanical and Industrial Engineering, University of Toronto, Toronto, ON M5S 3G8, Canada
e-mail: mandelis@mie.utoronto.ca

resolution. This diffusive limitation is inconsistent with efforts of several researchers to treat the frequency-domain heat diffusion equation as a hyperbolic Helmholtz equation with a complex wavenumber, defining wavefronts and applying Snell's refraction laws to thermal waves [1–4]. Others have adopted the hyperbolic Cattaneo–Vernotte's relativistic heat conduction equation [5]. While these interpretations seem to allow for wavefronts leading to depth-selective transfer of power by thermal waves, they both violate the second law of thermodynamics as they admit the propagation of energy against the field gradient (i.e., a temperature field in which heat would appear to be moving from cold to hot [6]). This article shows how non-propagating (parabolic) diffusion-wave energy fields can exhibit energy localization normally encountered in propagating hyperbolic wave fields without need for contradictory hyperbolic field assumptions, through a new thermal-wave binary phase code generation scheme and the subsequent matched filter signal processing using the parabolic diffusion-wave equation. Such a localized response from a diffusion-wave not only results in an improvement in axial resolution for thermal-wave imaging, but also allows for the deconvolution of individual responses of superposed axially discrete sources and leads to depth-selective rather than depth-integrated images. Potential diagnostic applications of this method include monitoring structural and mineralization changes in hard dental and bone tissues in a non-contact and safe manner. Conventional clinical diagnostic modalities lack sufficient sensitivity and/or specificity to detect early demineralization of hard tissues and mostly use ionizing radiation [7].

2 Experimental Apparatus and Procedures

In order to demonstrate depth selectivity, an experimental setup was built using a continuous-wave fiber-coupled 808 nm near-infrared laser illuminating the sample (Jenoptik, Jena, Germany), a mid-infrared camera focused on the interrogated surface of the sample (Cedip, Croissy-Beaubourg, France; Modeli: Titanium 520M, spectral range of 3.6 μm to 5.1 μm and frame rate of 370 Hz), a signal generation/acquisition device (National Instruments, Austin, Texas, NI-6229 BNC), and a four-axis sample positioning system [8–10]. The laser power was modulated sinusoidally by the signal generation device either at a fixed frequency (conventional lock-in thermography) or in a binary phase-coded manner to generate photothermal waves inside the sample. The data acquisition/signal processing program (designed in LabView environment) captures and averages the camera frames and their corresponding reference/modulation signal values. In the case of lock-in thermography, a standard two-dimensional (2D) quadrature demodulation was used to determine the amplitude and phase values of the thermal waves generated inside the sample [11]. For the case of binary phase-coded imaging, based on Eqs. 1a and 1b, the temporal infrared signal corresponding to each pixel, $s(t)$, was cross-correlated once with the modulation/reference signal, $f(t)$, and once with its quadrature. Subsequently, the cross-correlation (CC) and phase signals were calculated as shown in Fig. 1a.

$$\mathrm{CC}(l;\tau) = \varepsilon \times \Im^{-1}\left\{F(\omega)^* S(l;\omega)\right\}, \tag{1a}$$

$$\theta_{CC}(l) = \left. \frac{\mathcal{F} \times \Im^{-1}\{F(\omega)^* S(l;\omega)\}}{\mathcal{F} \times \Im^{-1}\left\{\left[-\mathrm{isgn}(\omega)F(\omega)\right]^* S(l;\omega)\right\}} \right|_{\tau=0}, \tag{1b}$$

where sgn(ω) is the signum function and the expression inside the square bracket in the denominator is the Fourier transform of the quadrature reference signal, experimentally obtained through the Hilbert and then Fourier transforms indicated in Fig. 1a. Note how the emissivity (ε) cancels out in the cross-correlation phase channel.

Depending on the contrast parameter chosen (the peak amplitude or its corresponding delay time, τ_p), two kinds of images can be produced from the cross-correlation signal: amplitude image or peak delay time τ_p image. Moreover, based on Eq. 1b, it is also possible to calculate the emissivity-normalized cross-correlation phase images. Cross-correlation matched filtering was introduced in the radar sciences in the early 1940s to detect deterministic signals within highly noised channels and to augment range resolution. This methodology localizes the energy of the received signal under a single peak located at a delay time (τ_p) equal to the delay between the transmitted and received signals. More energy localization can be achieved by means of pulse compression techniques such as frequency chirp or binary phase-coded modulation through reducing the width of the cross-correlation peak while increasing its height.

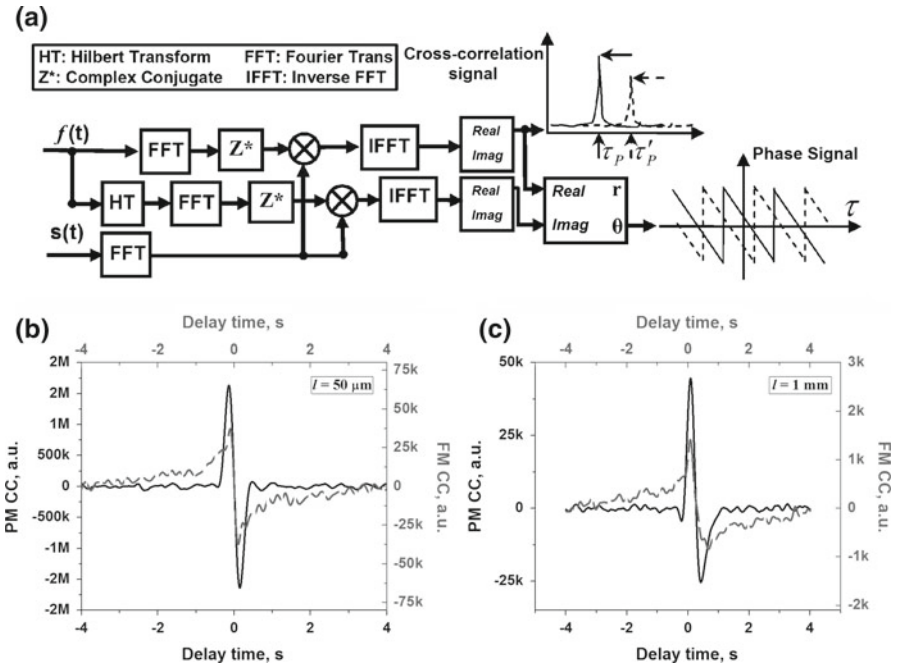

Fig. 1 (a) Signal processing block diagram of thermophotonic radar imaging. Theoretical simulation of cross-correlation signals using frequency (*dashed*) and phase (*solid*) modulation for absorbers at depths of (b) 50 μm and (c) 1 mm below the surface using thermal and optical properties of dental enamel. Frequency modulation: 0.1 Hz to 4.9 Hz, 6.4 s; Phase modulation: 2.5 Hz, 16 bit, 6.4 s

While frequency (chirp) modulation maintains a relatively constant power within the chirp frequency range (wide-band detection), phase modulation (i.e., binary phase coding) results in distinct energy localization advantages, especially with diffusive fields. Figure 1b, c plot theoretical comparisons of the cross-correlation signals obtained from frequency modulation (dashed lines) and phase modulation (solid lines) techniques. Optical and thermal properties of dental enamel were used for the turbid medium [10]. The cross-correlation responses clearly show that phase modulation significantly improves the axial resolution (full width at half maximum of the main peaks), as well as the signal-to-noise ratio (SNR). Moreover, the plots suggest that matched filtering using phase modulation can exhibit energy localization normally encountered in propagating hyperbolic wave fields. As a result, one can obtain localized information from absorbers at different depths by investigating the cross-correlation plots at the corresponding delay times or alternatively obtain iso-delay (iso-depth) images. Consequently, by scanning the image plane in the delay time axis, one can obtain what amounts to thermal coherence tomographic images and locally resolve axially superposed absorbers using the diffusion-wave field.

3 Results

Figure 2a schematically shows the cross section of a black plastic step wedge sample (step height = 200 μm) inside a scattering medium (polyvinyl chloride-plastisol with added titanium dioxide (TiO_2) powder to enhance scattering). Figure 2b shows

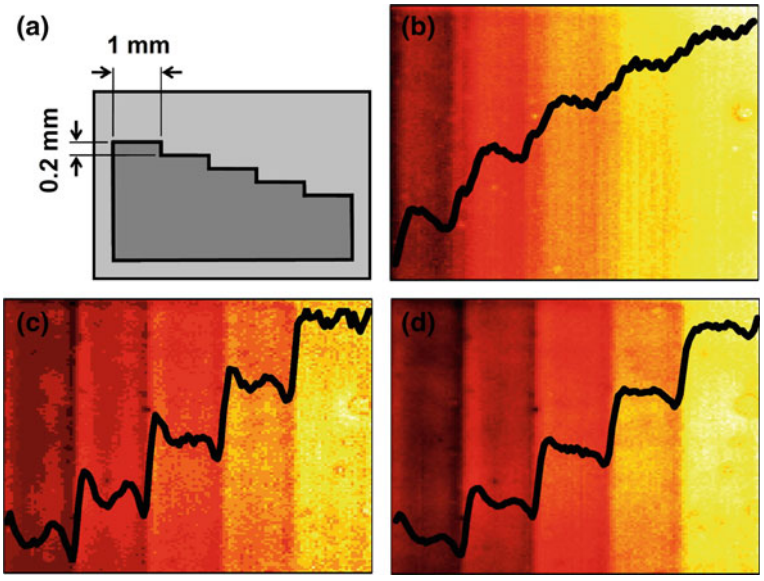

Fig. 2 (a) Cross section of the step wedge sample, (b) conventional lock-in thermography phase, (c) binary phase coding peak delay time, and (d) binary phase coding phase images of the step wedge sample using 16-bit [1 1 1 1 1 1 -1 1 -1 1 -1 -1 1 1 -1 -1] code. The *curve* in each image shows the mean horizontal profile of the corresponding contrast parameter

the conventional single frequency modulation phase image obtained at 3 Hz along with its mean profile over the steps. It can be seen that although lock-in imaging can detect all the steps, it loses its depth resolution over deeper steps due to the diffuse nature of thermal waves. On the other hand, binary phase-coded imaging at the same modulation frequency and experimental conditions (averaging, laser power, etc.), maintains excellent resolution down to the deepest step in both peak delay time and phase images, Fig. 2c, d, respectively. This experiment clearly shows how binary phase-coded matched filtering can result in a more localized response in a diffusive field and improve the axial resolution while probing deeply into the sample.

An illustration of the capabilities of thermal coherence tomography applied to turbid media (biological tissues) is its ability to detect early caries in human teeth which conventional clinical diagnostic modalities, like radiographs, cannot detect [8]. Early caries removes mineral from areas very close to the enamel surface and creates micro-pores which trap light photons, eventually promoting near-surface light absorption and thermal-wave generation. As a result, thermal waves from early caries travel less distance to reach the interrogated surface and yield higher amplitude and smaller phase lag/delay compared to those from intact regions. However, an important shortcoming of dental thermophotonic lock-in imaging is its inability to detect interproximal (in-between teeth) caries when inspected from the accessible buccal (front) surface. A comparison of lock-in thermography and binary phase-coded phase images in Fig. 3b, c under identical experimental conditions shows how the enhanced axial resolution of the binary phase-coded imaging can greatly enhance the contrast of deep interproximal caries. By constructing images at given delay times, one can perform depth-selective slicing in the turbid medium to resolve defective regions, Fig. 3e, from intact areas, Fig. 3f, a trait commonly shared with optical coherence tomography, but without the backscattering complications of optical coherence tomography which usually limit image dynamic range and optical coherence and penetration depths to the μm range.

Figure 4a shows the optical image of the interrogated surface of a goat bone along with its cross section. The optical image shows that the spongy trabecular bone is covered by the more dense cortical bone on the surface. Figure 4b, c shows the back surface of the sample before and after removing the trabecular structure, respectively. Similarly, Fig. 4d, e is the thermophotonic radar phase-modulated images obtained using the binary phase-coded technique before and after trabecular bone removal. The dashed circles indicate the location from which the trabecular bone was removed. Comparison of Fig. 4d, e clearly shows that depth-resolved binary phase-coded imaging reveals the trabecular structure that lies right below the cortical overlayer. Figure 4 suggests that another potential diagnostic application of the depth-selective thermophotonic radar imaging technology can be early bone osteoporosis imaging, provided that soft-tissue overlayers do not totally absorb the back-scattered thermal infrared radiation, or that the diffusive thermal-wave amplitude at the outer surface (skin) is measurable. Direct expenditures for treatment of osteoporotic fracture in the U.S. are estimated at $10 billion to $15 billion annually and no imaging methodology currently exists for the early diagnosis of osteoporosis.

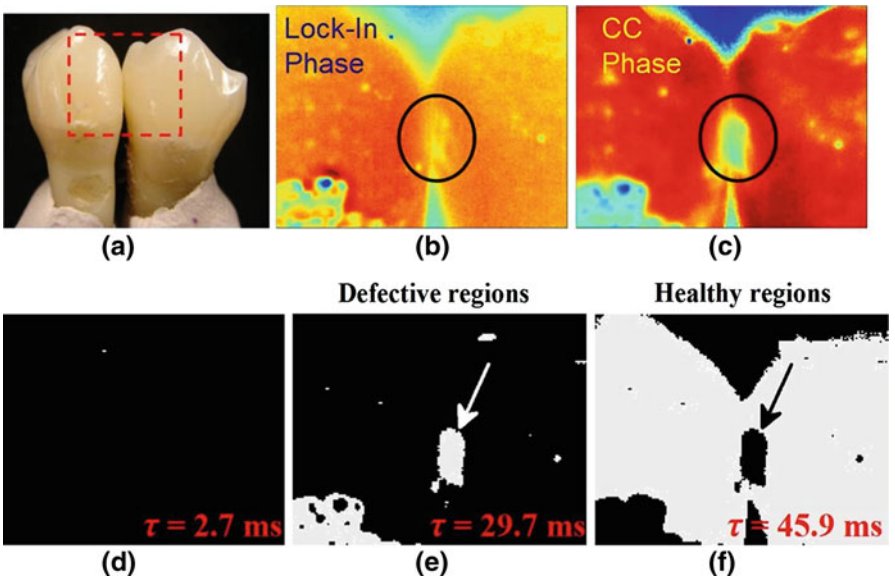

Fig. 3 (a) Teeth matrix with hidden inter-proximal early caries. The *rectangle* shows the imaged area. (b) Conventional lock-in thermography and (c) binary phase coding phase images of teeth matrix. (d–f) Depth-resolved thermal coherence tomographic images at several delay times (i.e., imaging depths)

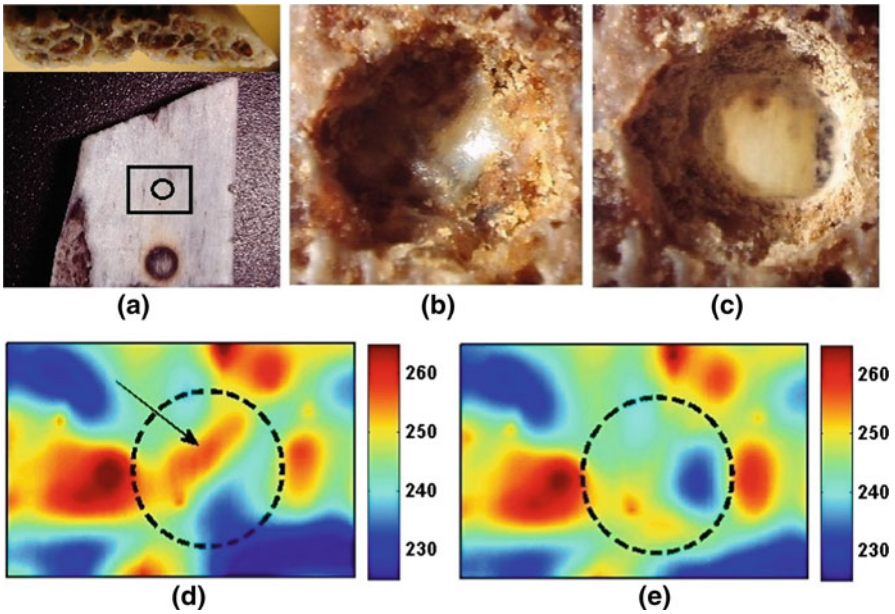

Fig. 4 (a) Optical image of the interrogated surface of a goat bone along with its cross section. The *rectangle* indicates the imaged area. Optical images of the back surface (b) before and (c) after the complete removal of the trabecular structure. Binary phase coding phase images (d) before and (e) after the complete removal of the trabecular structure. *Dashed circles* show the approximate location of the blind hole at the back

4 Conclusion

In conclusion, it has been shown theoretically and experimentally that the utilization of phase-modulated matched filtering (i.e., binary phase coding) in diffusion-wave fields yields a localized response from these normally depth-integrated parabolic fields which opens the way to depth-selective thermal coherence tomography. Potential applications cover a broad spectrum, including detecting and monitoring mineralization status of hard dental and bone tissues.

Acknowledgments We are grateful to the Ontario Ministry of Research and Innovation (MRI) for the 2007 (inaugural) Discovery Award in Science and Engineering to A.M., to the Canada Research Chairs Programs, the Federal and Provincial Governments for a CFI–ORF award, and the Natural Sciences and Engineering Research Council of Canada for several Discovery Grants to A.M.

References

1. M.A. O'Leary, D.A. Boas, B. Chance, A.G. Yodh, Phys. Rev. Lett. **69**, 2658 (1992)
2. J.A. Burt, Can. J. Phys. **64**, 1053 (1986)
3. D.P. Almond, P.M. Patel, *Photothermal Science and Techniques* (Chapman & Hall, London, 1996)
4. D.A. Boas, M.A. O'Leary, B. Chance, A.G. Yodh, Phys. Rev. E **47**, R2999 (1993)
5. J. Ordonez-Miranda, J.J. Alvarado-Gil, Int. J. Therm. Sci. **48**, 2053 (2009)
6. A. Mandelis, L. Nicolaides, Y. Chen, Phys. Rev. Lett. **87**, 020801 (2001)
7. S.C. White, M.J. Pharoah, Dental Caries, in *Oral Radiology*: *Principles and Interpretation* (Mosby, Toronto, 2004), pp. 297–313
8. N. Tabatabaei, A. Mandelis, B.T. Amaechi, J. Biomed. Opt. **16**, 071402 (2011)
9. N. Tabatabaei, A. Mandelis, B.T. Amaechi, Appl. Phys. Lett. **98**, 163706 (2011)
10. N. Tabatabaei, A. Mandelis, Phys. Rev. Lett. **107**, 165901 (2011)
11. O. Breitenstein, M. Langenkamp, *Lock-in Thermography: Basics and Use for Functional Diagnostics of Electronic Components* (Springer, New York, 2003)